Energy Conversion and Management 86 (2014) 233–240

Contents lists available at ScienceDirect

Energy Conversion and Management

journal homepage: www.elsevier.com/locate/enconman

Uninterrupted thermoelectric energy harvesting using temperature-sensor-based maximum power point tracking system

Jae-Do Park [a,*], Hohyun Lee [b], Matthew Bond [a]

[a] Department of Electrical Engineering, University of Colorado Denver, CB110, P.O. Box 173364, Denver, CO 80217, USA
[b] Department of Mechanical Engineering, Santa Clara University, 500 El Camino Real, Santa Clara, CA 95053, USA

ARTICLE INFO

Article history:
Received 27 January 2014
Accepted 7 May 2014
Available online 27 May 2014

Keywords:
Thermoelectric generator
Maximum power point tracking
Energy harvesting
Feedforward
Current sensorless

ABSTRACT

In this paper, a thermoelectric generator (TEG) energy harvesting system with a temperature-sensor-based maximum power point tracking (MPPT) method is presented. Conventional MPPT algorithms for photovoltaic cells may not be suitable for thermoelectric power generation because a significant amount of time is required for TEG systems to reach a steady state. Moreover, complexity and additional power consumption in conventional circuits and periodic disconnection of power source are not desirable for low-power energy harvesting applications. The proposed system can track the varying maximum power point (MPP) with a simple and inexpensive temperature-sensor-based circuit without instantaneous power measurement or TEG disconnection. This system uses TEG's open circuit voltage (OCV) characteristic with respect to temperature gradient to generate a proper reference voltage signal, i.e., half of the TEG's OCV. The power converter controller maintains the TEG output voltage at the reference level so that the maximum power can be extracted for the given temperature condition. This feedforward MPPT scheme is inherently stable and can be implemented without any complex microcontroller circuit. The proposed system has been validated analytically and experimentally, and shows a maximum power tracking error of 1.15%.

1. Introduction

Recently, investigation into sustainable alternative energy sources has been significantly expanded. In addition to the large-scale renewable energy systems using wind turbines and photovoltaic (PV) panels, the harvesting of small energy from various free energy sources, such as vibrations from a bridge, waste heat from internal combustion engines and brick kilns, and electricity from biological molecules, has been investigated in regard to direct power generation for low-power loads or system efficiency improvement through energy recovery [1,2]. Among these approaches, heat energy harvesting via thermoelectric generators (TEGs) converts thermal energy to electrical energy without any mechanical moving part. It is small, light, reliable, eco-friendly, and promising for applications such as automotive waste heat recovery and wireless sensor network power supply due to its long lifetime and high reliability [3–6]. Although it has suffered from low efficiency and high cost, the feasibility of TEG as an energy source is being improved by recent research progress in areas such as material efficiency [7–9] and energy harvesting system development [10,11].

While most research efforts have focused on enhancing thermoelectric material properties, power conditioning circuits optimized for TEG systems have not been investigated extensively. Many studies have suggested optimal electrical load matching conditions for maximized power generation, and utilized maximum power point tracking (MPPT) techniques originally developed for PV systems, such as Perturb and Observe (P&O) and Incremental Conductance (IC) [12–14]. Although maximizing the energy harvest from TEGs by means of an MPPT technique is essential for TEG applications to compensate the TEG's low conversion efficiency, conventional MPPT techniques for PV systems may not be optimal for TEG systems. Unlike a PV system, a TEG system requires a certain amount of time to reach a steady-state; hence, fast perturbations on output power in P&O and IC algorithms could lead to off-MPP operations due to the inaccurate instantaneous TEG power measurement. Moreover, these hill climbing techniques rely on fast measurements and complex computation, which in turn require additional hardware and software that consume measurable amount of power. The fractional voltage technique that samples the open circuit voltage (OCV) of the TEG while in operation is also widely used [15–17]. But, it also suffers from the large

* Corresponding author. Tel.: +1 (303) 352 3743; fax: +1 (303) 556 2383.
E-mail address: jaedo.park@ucdenver.edu (J.-D. Park).

http://dx.doi.org/10.1016/j.enconman.2014.05.027
0196-8904/

system time constant that is required to sample precise OCV for the given temperature differential. Furthermore, a microcontroller and analog switch are required to disconnect the TEG from the circuit and sample OCV, which can be costly and troublesome especially in low-power TEG systems.

In this paper, a temperature-sensor-based MPPT technique is proposed for TEG energy harvesting systems. The proposed system can track variations of MPP that are due to temperature changes with a simple and inexpensive temperature-sensor-based circuitry that can avoid the disadvantages of conventional techniques, such as current measurement, source disconnection, and power perturbation. Instead, TEG's OCV characteristic with respect to temperature difference between source and environment is built into the circuit; then a proper command voltage signal – i.e., half of the TEG's OCV for the given temperature differential – is generated. The command is used by a hysteresis controller to generate a gate signal for the power converter to harvest power from the TEG at the MPP of the given temperature condition without perturbation or interruption. The proposed MPPT circuitry can be implemented with a minimal number of discrete parts and without any complex microcontroller system. Moreover, the system is inherently stable because it operates based on the feedforward model without any instantaneous power feedback loop. The proposed scheme has been validated analytically and experimentally, and demonstrated successful performance.

2. TEG energy harvesting

2.1. Thermal model of thermoelectric module

Thermoelectric modules directly generate electricity proportional to the temperature difference applied across the legs. A typical schematic of a TEG system and its thermal circuit model is shown in Fig. 1. The heat flow in the system can be represented by the following two energy conservation equations.

$$\dot{Q}_H = \dot{Q}_{Cond} + \dot{Q}_{Peltier} - \dot{Q}_{JH} = \frac{T_S - T_H}{\Psi_H} \tag{1}$$

$$\dot{Q}_C = \dot{Q}_{Cond} + \dot{Q}_{Peltier} + \dot{Q}_{JH} = \frac{T_C - T_\infty}{\Psi_C} \tag{2}$$

where $\dot{Q}_H$ and $\dot{Q}_C$ denote the amount of heat transfer at the hot and cold surfaces of the thermoelectric module, $\dot{Q}_{Cond}$, $\dot{Q}_{Peltier}$, and $\dot{Q}_{JH}$ are heat conduction, Peltier heating/cooling, and Joule heating inside the thermoelectric material, respectively. ψ_H and ψ_C are the thermal resistance of the hot and cold sides. T_S, T_H, T_C, and T_∞ are the temperatures of the heat source, hot surface, cold surface, and ambient air, respectively. The energy conservation equations can be further expanded as

$$\dot{Q}_H = K(T_H - T_C) + \alpha I_{TEG} T_H - \frac{1}{2} I_{TEG}^2 R_{\text{int}} \tag{3}$$

$$\dot{Q}_C = K(T_H - T_C) + \alpha I_{TEG} T_C + \frac{1}{2} I_{TEG}^2 R_{\text{int}} \tag{4}$$

where K is the thermal conductance of TEG material, α is the Seebeck coefficient of TEG material, I_{TEG} is the TEG output current, and R_{int} is the internal electrical resistance of the TEG material [18]. The Seebeck coefficient and the internal resistance have been shown to be nearly constant over the operating range of the TEG [15]. The output power of the TEG module will be given as

$$P = \dot{Q}_H - \dot{Q}_C \tag{5}$$

Because $\dot{Q}_{Peltier}$ and $\dot{Q}_{JH}$ are functions of the TEG output current as can be seen in (3) and (4), the TEG output power will vary as the output current changes even with a constant temperature difference between T_H and T_C. Furthermore, T_H and T_C will also change with the amount of output current for the given source and ambient temperatures T_S and T_∞, because $\dot{Q}_H$ and $\dot{Q}_C$ are functions of the output current. So far, many thermoelectric system analyses have assumed that change of temperatures by electrical current is negligible, and have used a conventional maximum power output condition ($R_{int} = R_{ext}$). Several researchers addressed the inaccuracy of this approach in real applications and suggested new optimum operation conditions [18–21].

2.2. Electrical model and maximum power point

The electrical power converted from the thermal power by TEG will be given as

$$P = V_{TEG} I_{TEG} \tag{6}$$

where V_{TEG} and I_{TEG} are the voltage and current at TEG's output terminals, respectively. Taking into account the thermal factors described in Section 2.1, the TEG can be modeled as a dependent voltage source V_S with an internal resistance R_{int}, as shown in Fig. 2. The external resistance R_{ext} represents the electrical load that draws power from TEG.

The TEG will operate at a point on the V–I curve or power curve. It can also be associated with the load resistance seen by the TEG. In the conventional system model where the internal voltage V_s is constant and independent of output current, it can be analytically derived that the MPP occurs when $R_{int} = R_{ext}$ [15]. However, it has been shown that this impedance-matched MPP condition is valid only when the temperatures at both ends of the thermoelectric legs are kept constant [22,23]. This assumption cannot hold in practical applications, because temperatures at both ends of the

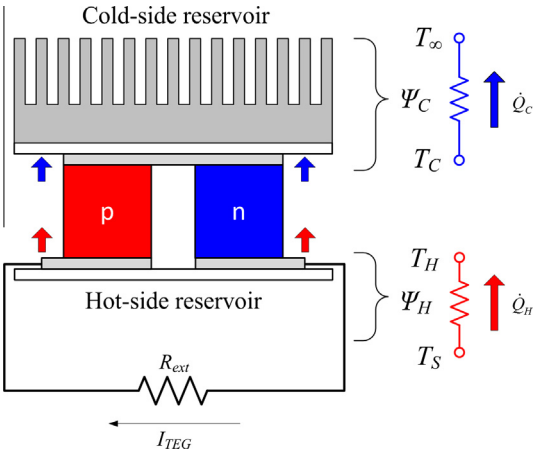

Fig. 1. Schematic and thermal circuit model of a typical thermoelectric module.

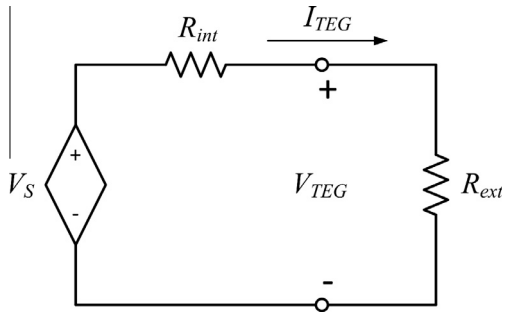

Fig. 2. Electrical equivalent circuit of TEG system.

thermoelectric legs that determine the internal source voltage in the equivalent circuit are affected by multiple factors, including conduction heat transfer through heat sink, energy transfer by Joule heating, the Peltier effect, and thermal conduction in the TEG module. Even for a constant temperature differential, the internal voltage will change as load current varies, which makes the MPP deviate from where the impedances are matched. For example, if V_s decreases as output current increases (V_{s2}), the V–I curve and power curve change from the constant V_s case (V_{s1}) and its MPP (MPP_2) will shift to where $R_{ext,} > R_{int}$, as shown in Fig. 3. However, it can be seen from the V–I lines that the MPPs are still at OCV/2.

New forms of load matching conditions have been suggested [18,19], but such conditions can only be applied when system parameters, such as heat sink or geometry of TEG, are carefully chosen. Moreover, load conductance is difficult to match when a non-constant electric load is directly connected; however, because the V–I curve is near linear for most applications [24,25], especially when source temperature is kept constant [26], the MPP will be at half of the OCV regardless of R_{ext}/R_{int} relationships.

2.3. Conventional MPPT techniques

The Perturb and Observe (P&O) technique is widely used in TEG applications as well [27–29]. It samples the instantaneous power production of the generator after a perturbation at discrete intervals on either side of the current operating point, and moves the operating point toward that of higher power; however, the P&O technique responds poorly to a fast-changing power output [30] and it is inefficient at the steady state due to the fact that the constant perturbation/sampling and high-frequency fluctuation of the operating point cause a harmonic around the MPP [31].

Incremental conductance (IC) is a method that can avoid the oscillations at MPP in P&O systems [32]. The IC method compares the incremental conductance ($G_d = dI/dV$) of the generator against the negative value of instantaneous conductance ($G_s = -I/V$). At any point on the power curve before the MPP, G_d is greater than G_s and the operational point is moved toward the higher voltage. At an operating point after the MPP, G_s is greater than G_d and the operational point is moved toward a lower voltage. The MPP is reached when $G_d = G_s$, and IC does not search unless there is a change in current. The IC algorithm shows better performance in terms of noise and system dynamics compared to P&O, but worse in rapidly changing source conditions, and there would be a stability issue with a high perturbation rate [33]. Like the P&O techniques, this perturbation-based approach is not suitable for TEG applications due to TEG's slow response to the power perturbation.

The virtual conductance measurement technique uses voltage and current measurements to calculate instantaneous load conductance ($G_O = I_{TEG}/V_{TEG}$) and compare it to the pre-determined internal conductance ($G_I = 1/R_{int}$) to find the MPP [34]. The power converter controls the TEG output voltage V_{TEG} to operate at the load matching condition; however, as shown in Fig. 3, this approach cannot be applied to the system that the internal voltage source changes as output current varies because the load matching is not the MPP condition.

The fractional OCV method uses the relationship between MPP voltage and OCV [16,17,35]. The OCV is sampled periodically to determine the MPP voltage for the given condition; however, the power source should be electrically disconnected by a switch or by shutting off the power converter for the OCV measurement while in operation. Hence, temporary power loss and complex implementation are drawbacks if this approach. For TEG applications, the large time constant of the temperature change would also be problematic for precise OCV measurement.

3. Proposed MPPT system

In this paper, a model-based MPPT controller that estimates OCV using two temperature measurements is developed to avoid the aforementioned disadvantages of conventional techniques. The proposed system determines the operating point at MPP, which is half of the OCV, in a feedforward manner using temperature measurements without any feedback information of actual power or output resistance. This results in continuous power harvesting at MPP that does not require any perturbation or interruption. Furthermore, complex hardware and software requirements and complicated thermal-electrical considerations are not necessary, because the MPP is at half of the OCV for most of the applications due to the linear V–I characteristics.

3.1. OCV estimation using temperature measurements

From the thermal model shown in Fig. 1, temperature drop across thermoelectric legs in the open circuit condition when $I_{MFC} = 0$ can be obtained as follows.

$$(T_H - T_C)_{OC} = \frac{1/K}{\Psi_H + \Psi_C + 1/K}(T_s - T_\infty) = \frac{(T_s - T_\infty)}{K\Psi_H + K\Psi_C + 1} \tag{7}$$

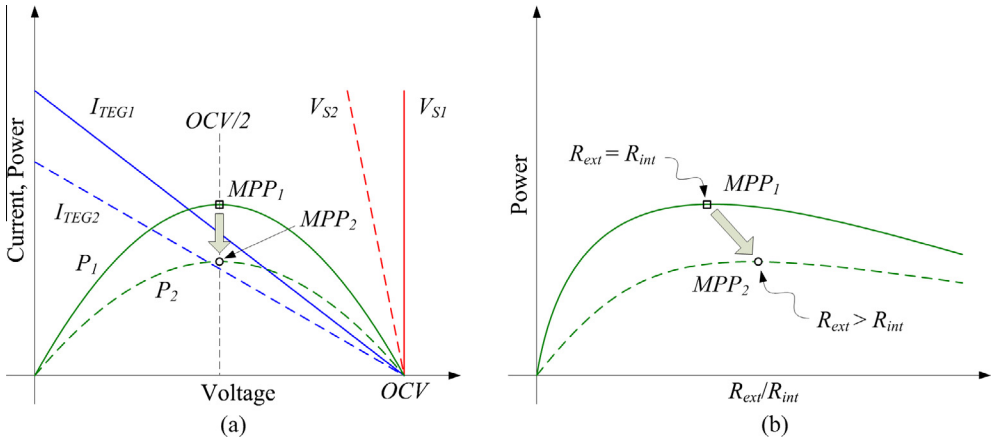

Fig. 3. Comparison of operations with constant (V_{S1}) and output-current-dependent (V_{S2}) internal voltage source for a given temperature difference between both ends of thermoelectric legs. It can be seen that the MPP_2 shifts to where $R_{ext} \neq R_{int}$, but still occurs at OCV/2. (a) TEG output currents and power vs. TEG output voltage. (b) Output power vs. R_{ext}/R_{int} ratio.

The OCV is directly proportional to the temperature difference at the open circuit condition, and the proportional coefficient will be the Seebeck coefficient S of a TEG module.

$$V_{OC} = S(T_H - T_C)_{OC} = \frac{S(T_s - T_\infty)}{K\Psi_H + K\Psi_C + 1} \tag{8}$$

The thermal resistances depend on contact resistances, pad resistance, and heat sinks, among others, but these values are quite difficult for end users to evaluate and must be identified through calibration. The Seebeck coefficient S of a TEG module that contains N p- and n-type legs will be given as $N\alpha$, where α is the material Seebeck coefficient.

It can be seen from (7) that the OCV can be represented as a linear function of external temperatures of T_S and T_∞.

$$V_{OC} = \kappa(T_s - T_\infty) \tag{9}$$

where κ is the proportional constant, which depends on thermal resistances and module properties. Although it is difficult to analytically calculate κ because module properties are not usually provided by TEG manufacturers, the constant κ can be readily determined experimentally by measuring OCV for the given temperature differences between T_S and T_∞. It does not depend on the output current because it is measured in no-load conditions. Furthermore, T_S and T_∞ are easily accessible unlike T_H and T_C.

3.2. Feedforward MPPT controller for uninterrupted energy harvesting

The proposed MPPT controller, i.e., a TEG model/MPP reference generator, implements an energy harvesting system in conjunction with a hysteresis controller to generate a power converter gate signal and a boost converter for energy capture. The proposed energy harvesting system extracts and stores the maximum attainable energy for the given operating conditions. A schematic of the overall system is shown in Fig. 4.

TEG's OCV is linear in terms of temperature differential as can be seen in (9), and it has been shown that MPP is at half of the OCV. The reference voltage for MPP will therefore be

$$V_{REF} = \frac{\kappa}{2}(T_s - T_\infty) = \frac{\kappa}{2}\Delta T \tag{10}$$

This TEG model – i.e., OCV vs. temperature difference – can easily be modeled with a differential amplifier and temperature sensors as shown in Fig. 4, which enables a feedforward tracking of the MPP based on instantaneous temperature measurements. The output voltage of the model circuit is given as follows:

$$V_{REF} = \frac{R_2}{R_1}\Delta V_T \tag{11}$$

where ΔV_T is the voltage difference of temperature sensor output for T_S and T_∞ (i.e., $V_{HOT} - V_{COLD}$). Using a circuit with potentiometers, the OCV characteristic of any TEG module can be modeled, and the OCV/2 for any temperature differential can be readily generated for the power conversion stage. The temperature measurement circuit is much easier to implement and less expensive than the ones used for current measurement or TEG disconnection which require a microcontroller system for A/D conversion and MPPT algorithm implementation, which is a significant advantage especially for low-power systems. Continuous power harvesting without any perturbation or interruption would also be a substantial advantage of the proposed scheme for TEG applications that have a large time constant for temperature changes. Moreover, it can be implemented with an OP amp and four resistors, which is much simpler than the conventional microcontroller-based MPP searching algorithms.

To maintain the TEG output voltage at the commanded MPP, the hysteresis-controller-based gate drive circuitry is used [36,37]. The hysteresis control circuit generates an appropriate gating signal so that the power converter can maintain the TEG output voltage V_{TEG} at the reference voltage of the given temperature condition, which tracks the varying MPP. A hysteresis controller can easily be implemented with a comparator and two resistors, as shown in Fig. 4.

The hysteresis controller has two thresholds (V_{ThH} and V_{ThL}) generated by V_{REF} to compare with the input voltage V_{TEG}.

$$V_{ThH} = \frac{R3 + R4}{R4}V_{REF} - \frac{R3}{R4}V_{oL} \tag{12}$$

$$V_{ThL} = \frac{R3 + R4}{R4}V_{REF} - \frac{R3}{R4}V_{oH} \tag{13}$$

where V_{REF} is the output voltage of the TEG model circuit, which is OCV/2 for the given temperature difference, and V_{oH} and V_{oL} are the

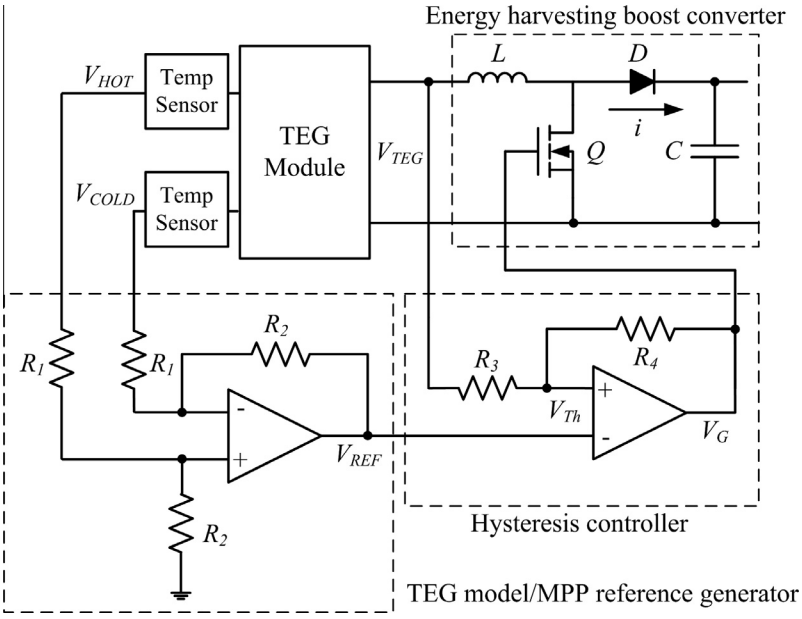

Fig. 4. Overall schematic of the proposed energy harvesting system. TEG model feeds the hysteresis controller with an MPP voltage reference. Hysteresis controller controls boost converter and maintains energy harvesting at MPP.

high and low voltage of the comparator's binary output V_G, respectively. When the TEG output voltage reaches the upper threshold V_{ThH}, the hysteresis controller turns on the main power MOSFET Q in the boost converter, ($V_G = V_{oH}$, logic high), to start extracting power from the TEG. In this mode, V_{TEG} decreases as output current increases and the energy is stored in the inductor of the boost converter. When the V_{TEG} hits the lower threshold V_{ThL}, the hysteresis controller turns off Q ($V_G = V_{oL}$, logic low) and the extraction stops. Then, energy stored in the inductor is discharged to the output capacitor. In this mode, V_{TEG} increases and when it is recovered to V_{ThH}, the extraction resumes. The output of the hysteresis controller can be seen in Fig. 5. The high and low logic levels of V_G to turn on and off the power switch can vary by circuit configuration.

If we pick an $R4$ value significantly larger than $R3$ ($R4 \gg R3$), the thresholds will be given as follows for a general comparator with a dual power supply ($-V_{sat} \leqslant V_o \leqslant V_{sat}$).

$$V_{ThH} = V_{REF} + \frac{R3}{R4} V_{sat} \tag{14}$$

$$V_{ThL} = V_{REF} - \frac{R3}{R4} V_{sat} \tag{15}$$

The control circuit can be much simpler if a single supply comparator ($0 \leqslant V_o \leqslant V_{sat}$) is used. Then, the upper threshold becomes

$$V_{ThH} = V_{REF} \tag{16}$$

The gate signal V_G changes between zero and V_{SAT} if the circuit is implemented with a single supply op amp.

By repeating these two operational modes, V_{TEG} can be confined in the band between V_{ThH} and V_{ThL} around MPP. The periods of these two modes, as well as the switching frequency, are determined by the TEG output power and power converter parameters. The operation of the TEG with a hysteresis controller is shown in Fig. 6.

4. Results and discussion

4.1. Experimental setup

A diode-based boost converter is selected for the energy harvesting experiment in this paper due to its simplicity, but any type of power converter can be integrated with the proposed control scheme. A low-power single-supply operational amplifier (LM392N, Texas Instruments, TX), a low-power comparator (MCP6542, Microchip Technology, AZ), and generic resistors and potentiometers have been used to implement feedforward TEG model and a hysteresis controller, respectively. For the boost converter, a 450μH inductor (RC-7, Triad Magnetics, CA), an N-channel MOSFET (NTD4906N-35G, ON Semiconductor, AZ), a Schottky diode (BAT46, STMicroelectronics, Switzerland), and a 3F, 2.5 V supercapacitor (M1020-2R5305-R, Cooper Bussmann, MO) were

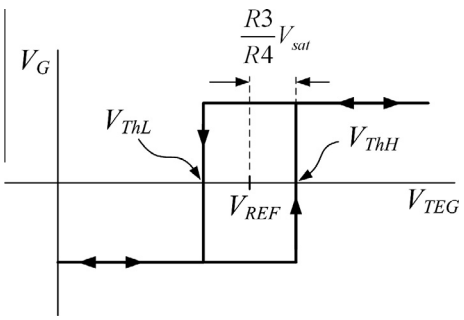

Fig. 5. Thresholds V_{ThH}, V_{ThH} and output V_G of hysteresis controller.

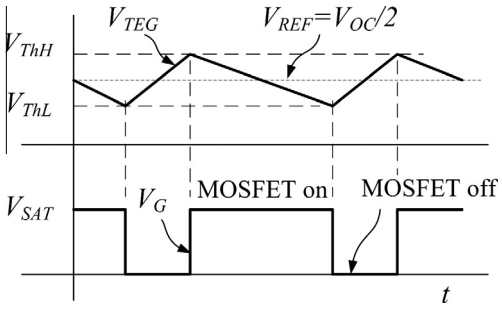

Fig. 6. TEG operation at MPP with hysteresis controller.

used. A generic potentiometer (1 MΩ) was used to control the load current. The implemented MPPT control circuit and power converter can be seen in Fig. 7.

The hot side of the TEG module was mounted on an aluminum block on a temperature-controlled hotplate (HP131225Q, Thermo Scientific, MA), and the cold side was attached to a generic CPU cooling heat sink/fan assembly. A fire brick was inserted between the hotplate and the heat sink to minimize the effect of convection heat. For temperature measurement, temperature sensors (MCP9700, Microchip Technology, AZ) were used. MCP9700 has a linear temperature slope (10 mV/°C) over the whole operating range unlike thermistors and significantly higher output voltage (1.75 V at 125 °C) than thermocouples. Furthermore, this sensor has good measurement accuracy (±4 °C max) and draws low current (6 μA typical), so it can be readily used for low-temperature-difference and low-power TEG applications. Thermal compound (RG-ICFN-200G-B1, Cooler Master, CA) and thermal adhesive (ASTA-7G, Arctic Silver, CA) were used for the TEG and temperature sensor mount, respectively. A current meter (AEMC K110, Chauvin Arnoux, NH) with a 10 mV/mA gain was used to measure the TEG output current. Two thermocouples and multimeters were used to measure temperatures; these measurements were for reference and were not used for control. For the experiments in this paper, a Bi-Te based TEG module (G2-30-0313, Tellurex, MI) was used. The experimental setup is shown in Fig. 8.

4.2. Results

To determine the TEG model circuit parameters, the experimental TEG system's OCV in terms of the temperature difference ΔT

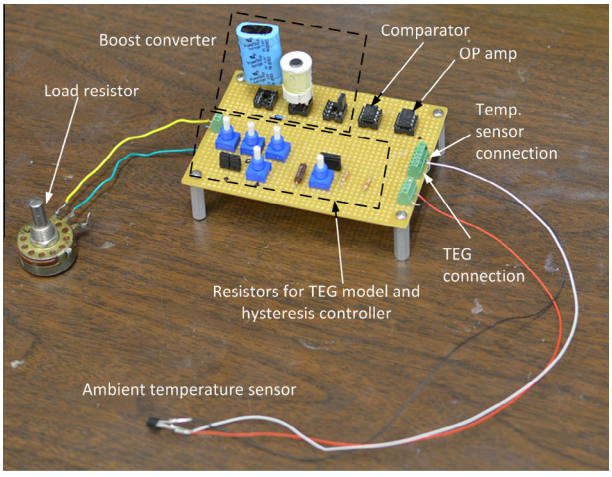

Fig. 7. Energy harvesting system: MPPT controller, hysteresis controller, and power converter. Load resistor and ambient temperature sensor are also shown.

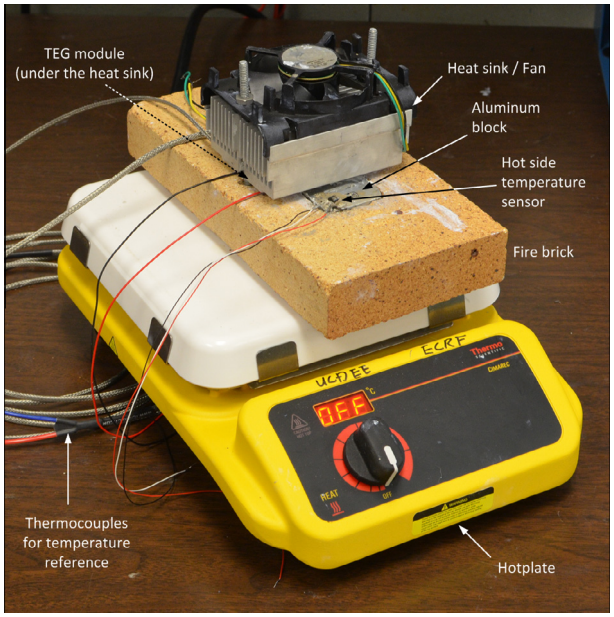

Fig. 8. Experimental setup.

between T_S and T_∞ was characterized, and the result is shown in Fig. 9. A linear characteristic can be seen as expected in (9), and the coefficient κ was found to be 0.0154 [V/°C]. The OCV characteristic with respect to the temperature sensor output was also measured, and it is characterized as

$$V_{OC} = 0.74\Delta V_T \tag{17}$$

where ΔV_T is the output voltage difference of temperature sensors for T_S and T_∞. Hence, the command voltage for the MPP of the given voltage differential (i.e., temperature differential) will be given as follows:

$$V_{CMD} = 0.5 \times V_{OC} = 0.37\Delta V_T \tag{18}$$

The command voltage is also shown in Fig. 9. This TEG's MPP characteristic in terms of the sensor output voltage difference is implemented in the model circuit using 20 kΩ and 7.42 kΩ for R_1 and R_2, respectively. These two resistances are the only parameters to be determined for TEG model. Although any resistance values can be selected as long as the ratio is maintained, higher values would be preferable due to low power consumption.

The *V–I* characteristic of the overall system is identified for different load and temperature conditions. Five different temperature conditions were given: ΔT = 17 °C, 45 °C, 79 °C, 95 °C and 122 °C. The source temperature was regulated by the hotplate, and ambient temperature change was negligible during testing. Around 15 data points were taken in load current range from 0 to 600 mA, and enough time was given to stabilize the output. Data points and linear regression lines can be seen in Fig. 10. The linear expressions for each *V–I* characteristic are shown in Table 1, and OCVs estimated from *V–I* characteristics are compared to experimentally measured ones to verify the expressions.

The proposed MPPT scheme was tested with the same temperature conditions that were used for *V–I* characterization. When the temperature condition is changed, the TEG model is supposed to feed the appropriate command voltage (i.e., MPP voltage for the new temperature differential) to the hysteresis controller so that the power converter can always extract the maximum power in any temperature condition. The performance of the proposed system has been verified by monitoring instantaneous waveforms of TEG output voltage and current, the output signal of the hysteresis controller, and the power converter output voltage using a digital oscilloscope. A screen capture for the operation when ΔT = 17 °C is shown in Fig. 11. It can be seen that the TEG is operating at 157 mV (CH1) and 70.5 mA (CH3, 1 mA/10 mV), which is the MPP for the given temperature condition. The operations at other temperature conditions were measured in the same manner, and the result of MPPT operation is shown along with the voltage-power curves generated from *V–I* characteristics in Fig. 12. The solid dots denote the operating points controlled by the proposed controller at each given temperature condition, and comparisons to the calculated operating conditions from the *V–I* expressions are shown in Table 1. Clearly, the proposed controller tracks the varying MPP fairly well.

The hysteresis voltage band was set to 100 mV using a fixed 30 Ω resistor and 3.25 MΩ potentiometers for R_3 and R_4, respectively. It should be noted that the band could be larger than the theoretical value because of the propagation delay of the comparator.

4.3. Discussion

The MPPT circuit suggested in this paper estimates OCV from source and ambient temperatures that can be easily measured and extracts energy at half of the estimated OCV. One of the advantages of the proposed technique over other MPPT algorithms is that it can be implemented with much less energy consumption and complexity. As the power and voltage generated from a TEG module are quite small, even a small voltage drop and power loss across the shunt resistor can be detrimental and may not be economically justified. The same is true of any additional power consumption by complex power management circuit using A/D converter and microcontroller. Although the MPPT systems based on the conventional fractional voltage is fast and reliable, the technical challenge

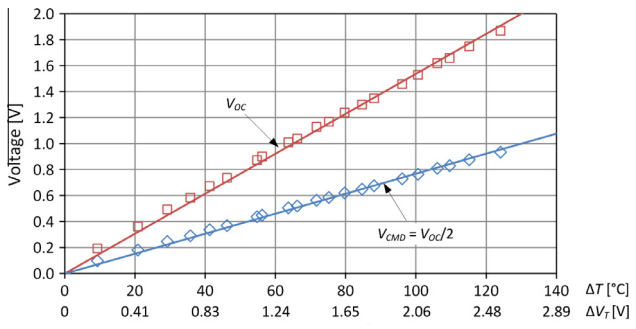

Fig. 9. Experimental OCV measurement with respect to temperature difference and temperature sensor output voltage difference between T_S and T_∞. Command voltage for power converter controller, OCV/2, is also shown.

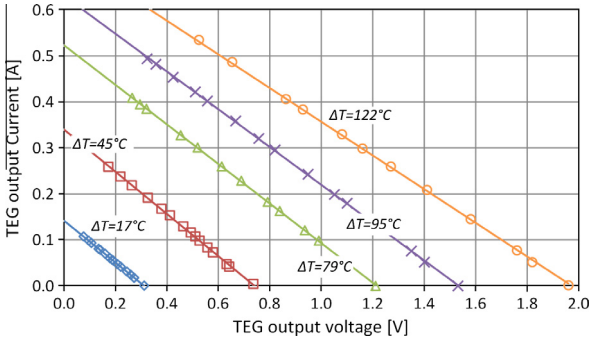

Fig. 10. *V–I* characteristics of the TEG used in this paper with different load and temperature conditions.

Table 1
Experimental result: (1) *V–I* characterizations. (2) OCV measurements. $\widehat{V}_{OC}$: estimated OCV from *V–I* curve expression, V_{OC}: experimentally measured OCV. (3) Operating point comparisons. $\widehat{V}_{TEG}$, $\widehat{I}_{TEG}$ and $\widehat{P}$: calculated output current and power at MPP from *V–I* characteristics. V_{TEG}, I_{TEG} and P: actual TEG output voltage, current, and power controlled by the proposed system. (4) Performance. V_{ERR} and P_{ERR} denote the error between $\widehat{V}_{TEG}$ and V_{TEG}, $\widehat{P}_{TEG}$ and P_{TEG}.

ΔT (°C)	System characterization	OCV measurements			Calculated operating point			Actual operating point			Performance	
	V–I curve expression (mA, mV)	$\widehat{V}_{OC}$ (mV)	V_{OC} (mV)	Err (%)	$\widehat{V}_{TEG}$ (mV)	$\widehat{I}_{TEG}$ (mA)	$\widehat{P}$ (mW)	V_{TEG} (mV)	I_{TEG} (mA)	P (mW)	V_{ERR} (%)	P_{ERR} (%)
17	$i = -0.4547v + 141.83$	312.0	311.0	0.32	155.0	70.9	11.1	157.0	70.5	11.1	−1.29	0.08
45	$i = -0.4587v + 339.78$	740.8	735.0	0.78	367.5	169.9	62.9	370.0	172.0	63.6	−0.68	1.15
79	$i = -0.4301v + 523.05$	1216.2	1210.0	0.51	605.0	261.5	159.0	615.0	258.5	159.0	−1.65	−0.03
95	$i = -0.4505v + 629.95$	1534.6	1530.0	0.30	765.0	315.0	241.7	769.0	316.0	243.0	−0.52	0.55
122	$i = -0.3661v + 722.39$	1973.2	1960.0	0.67	986.6	361.2	356.4	986.6	365.0	358.5	0.36	0.68

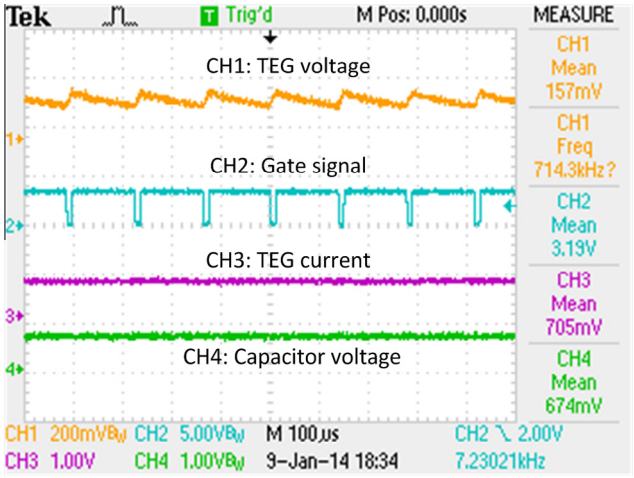

Fig. 11. Instantaneous TEG voltage, current, power converter gate signal, power converter. TEG current (CH3) is measured with 1 mA/10 mV current probe. The TEG is operating at 157 mV (CH1) and 70.5 mA (CH3, 1 mA/10 mV), which is the MPP for the given temperature condition.

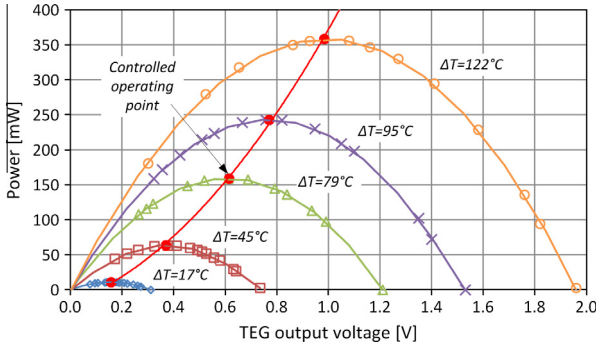

Fig. 12. Experimental result of MPPT control. Solid dots denote the controlled operating points by the proposed system at each given temperature condition.

lies in how to determine OCV efficiently. Commercially available OCV-based MPPT circuits periodically cut electrical current from TEGs and sample OCV, which has critical issues with TEGs. If current is interrupted for a short period in order to achieve a faster tracking performance, it may not be long enough for TEGs to reach thermal equilibrium and correct OCV. Similarly, P&O and IC methods have the same issue as the temperature cannot respond quickly enough to the perturbations. The change in power after perturbation can be instantaneously larger than its steady-state value. It could even take a few minutes for some systems to reach a steady-state, and such long disconnection is not desirable for energy harvesting applications.

The proposed feedforward model and the hysteresis controller can be implemented with a minimal number of discrete parts, and the system can be further simplified if the amplifier and comparator are built into a single chip. The proposed scheme does not require any current measurement or complex microcontroller system, which makes the proposed scheme very straightforward, cost-effective, and reliable. Although only an energy harvesting converter that captures the maximum available energy from TEG was built in this study, a secondary power converter can easily be implemented for the additional output voltage control, such as constant voltage output or battery charging, to provide more flexible operation.

The suggested circuit can steadily find an MPP even when the energy harvester is exposed to unstable source/ambient temperature, such as waste heat recovery from a cook stove or a wearable energy harvester, as well as under controlled cooling conditions. One should note that the proposed circuit responds to the change in source/ambient temperatures and cannot track the MPP variation due to the change of κ, the heat dissipation characteristic of the energy harvesting system; however, although the convective heat transfer coefficient is a function of temperature, the overall change in κ is not significant for stationary applications. A new MPPT strategy for varying heat dissipation characteristics is currently under investigation.

5. Conclusion

In this paper, a temperature-sensor-based MPPT technique has been proposed for TEG energy harvesting systems. The presented system operates based on the reference voltage for MPP generated by the feedforward TEG OCV model. The proposed MPPT scheme can track the MPP of any TEG system without current measurement, power perturbation or source disconnection, which enables optimal energy harvesting at any temperature or load condition with a much simpler and much less expensive circuitry. The MPPT scheme can be implemented with a minimal number of discrete parts and requires no complex hardware or software. Moreover, it is inherently stable because the system has no instantaneous power measurement feedback loop and can readily be used in conjunction with any type of power converter. The proposed scheme has been validated analytically and experimentally, and demonstrated successful performance.

References

[1] Hamilton M. Recent advances in energy harvesting technology and techniques. In: IECON 2012 – 38th Annual conference on IEEE industrial electronics society, Montreal; 2012.
[2] Vullers R, Schaijk R, Doms I, Hoof CV, Mertens R. Micropower energy harvesting. Solid-State Electron 2009;53:684–93.
[3] Karri M, Thancher E, Helenbrook B. Exhaust energy conversion by thermoelectric generator: two case studies. Energy Convers Manage 2011;52(3):1596–611.
[4] Yang J, Stabler F. Automotive applications of thermoelectric materials. J Electron Mater 2009;38(7):1245–51.
[5] Yongming Shi YW, Deng Y, Gao H, Lin Z, Zhu W, Ye H. A novel self-powered wireless temperature sensor based on thermoelectric generators. Energy Convers Manage 2014;80:110–6.

[6] Bonin R, Boero D, Chiaberge M, Tonoli A. Design and characterization of small thermoelectric generators for environmental monitoring devices. Energy Convers Manage 2013;73:73–81.
[7] Hsu FK, Loo S, Guo F, Chen W, Dyck J, Uher C, et al. Cubic AgPbmSbTe2+m: bulk thermoelectric materials with high figure of merit. Science 2004;303(5659):818–21.
[8] Dresselhaus MS, Chen G, Tang M, Yang R, Lee H, Wang D, et al. New directions for low-dimensional thermoelectric materials. Adv Mater 2007;19:1043–53.
[9] Heremans JP, Jovovic V, Toberer E, Saramat A, Kurosaki K, Charoenphakdee A, et al. Enhancement of thermoelectric efficiency in PbTe by distortion of the electronic density of states. Science 2008;321(5888):554–7.
[10] Saqr K, Musa M. Critical review of thermoelectrics in modern power generation applications. Therm Sci 2009;13(3):165–74.
[11] Ramadass Y, Chandrakasan A. A battery-less thermoelectric energy harvesting interface circuit with 35 mV startup voltage. IEEE J Solid-State Circuits 2011;46(1):333–41.
[12] Phillip N, Maganga O, Burnham K, Ellis M, Robinson S, Dunn J, et al. Investigation of maximum power point tracking for thermoelectric generators. J Electron Mater 2013;42(7):1900–6.
[13] Kim R-Y, Lai J-S. A seamless mode transfer maximum power point tracking controller for thermoelectric generator applications. IEEE Trans Power Electron 2008;23(5):2310–8.
[14] Kim J, Kim C. A DC–DC boost converter with variation-tolerant MPPT technique and efficient ZCS circuit for thermoelectric energy harvesting applications. IEEE Trans Power Electron 2013;28(8):3827–33.
[15] Kim S, Cho S, Kim N, Park J. A maximum power point tracking circuit of thermoelectric generators without digital controllers. IEICE Electron Exp 2010;7(20):1539–45.
[16] Montecucco A, Siviter J, Knox AR. Simple, fast and accurate maximum power point tracking converter for thermoelectric generators. In: 2012 IEEE energy conversion congress and exposition (ECCE); 2012.
[17] Schwartz DE. A maximum-power-point-tracking control system for thermoelectric generators. In: 2012 3rd IEEE international symposium on power electronics for distributed generation systems (PEDG); 2012.
[18] Yazawa K, Shakouri A. Optimization of power and efficiency of thermoelectric devices with asymmetric thermal contacts. J Appl Phys 2012;111(2). 024509-024509-6.
[19] McCarty R. Thermoelectric power generator design for maximum power: it's all about ZT. J Electron Mater 2013;42(7):1504–8.
[20] Freunek M, Muller M, Ungan T, Walker W, Reindl L. New physical model for thermoelectric generators. J Electron Mater 2009;38(7):1214–20.
[21] Gomez M, Reid R, Ohara B, Lee H. Influence of electrical current variance and thermal resistances on optimum working conditions and geometry for thermoelectric energy harvesting. J Appl Phys 2013;113(17). pp. 174908, 174908-8.
[22] Angrist S. Direct energy conversion. 4th ed. Allyn and Bacon: Boston, MA; 1982.
[23] Rowe M. CRC handbook of thermoelectrics. Boca Raton, FL: CRC Press; 1995.
[24] Decher R. Direct energy conversion – fundamentals of electric power production. NY: Oxford University Press; 1997.
[25] Laird I, Lu D. High step-Up DC/DC topology and MPPT algorithm for use with a thermoelectric generator. IEEE Trans Power Electron 2013;28(7):3147–57.
[26] Yoon N, Lee H, Wee DGM, Reid R, Ohara B. Achieving maximum power in thermoelectric generation with simple power electronics. J Electron Mater 2013.
[27] Vadstrup C, Schaltz E, Chen M. Individual module maximum power point tracking for thermoelectric generator systems. J Electron Mater 2013;42(7):2203–8.
[28] Yu C, Chau K. Thermoelectric automotive waste heat energy recovery using maximum power point tracking. Energy Convers Manage 2009;50(6):1506–12.
[29] Eakburanawat J, Boonyaroonate I. Development of a thermoelectric battery-charger with microcontroller-based maximum power point tracking technique. Appl Energy 2006;83(7):687–704.
[30] Ibrahim H, Ibrahim M. Comparison between fuzzy and P&O control for MPPT for photovoltaic system using boost converter. J Energy Technol Policy 2012;2(6):1–11.
[31] Hohm DP, Ropp ME. Comparative study of maximum power point tracking algorithms. Progr Photovoltaics: Res Applic 2003;11(1):47–62.
[32] Enslin J. Maximum power point tracking: a cost saving necessity in solar energy systems. Renew Energy 1992;2(6):543–9.
[33] Elgendy M, Zahawi B, Atkinson D. Assessment of the incremental conductance maximum power point tracking algorithm. IEEE Trans Sust Energy 2013;4(1):108–17.
[34] Zhang X, Chau K. An automotive thermoelectric–photovoltaic hybrid energy system using maximum power point tracking. Energy Convers Manage 2011;52(1):641–7.
[35] Ahiska R, Mamur H. A test system and supervisory control and data acquisition application with programmable logic controller for thermoelectric generators. Energy Convers Manage 2012;64:15–22.
[36] Alaraj M, Ren Z, Park J-D. Microbial fuel cell energy harvesting using flyback converter. J Power Sources; 2013. doi: 10.1016/j.jpowsour.2013.09.017 [in press].
[37] Park J-D, Ren Z. Energy harvesting system for microbial fuel cells with maximum power point and parallel operation capability. IEEE Trans Energy Convers 2012;Vol 27(3):715–24.